JGR Oceans

Key Points:
- CESM2 (CESM1-LE) snow depths on Arctic sea ice are thinner (thicker) than observed depths
- The 1950–2050 trends in annual mean snow depth on Arctic sea ice are −0.8 and −3.6 cm decade^{-1} in CESM2 and CESM1-LE, respectively
- CESM2 shows enhanced earlier snowmelt, less snow accumulation, more sublimation, and slightly more snow-ice formation in future decades

Correspondence to:
M. A. Webster,
mwebster3@alaska.edu

Snow on Arctic Sea Ice in a Warming Climate as Simulated in CESM

M. A. Webster[1] , **A. K. DuVivier[2]** , **M. M. Holland[2]** , and **D. A. Bailey[2]**

[1]Geophysical Institute, University of Alaska Fairbanks, Fairbanks, AK, USA, [2]National Center for Atmospheric Research, Boulder, CO, USA

Abstract Earth system models are valuable tools for understanding how the Arctic snow-ice system and the feedbacks therein may respond to a warming climate. In this analysis, we investigate snow on Arctic sea ice to better understand how snow conditions may change under different forcing scenarios. First, we use in situ, airborne, and satellite observations to assess the realism of the Community Earth System Model (CESM) in simulating snow on Arctic sea ice. CESM versions one and two are evaluated, with V1 being the Large Ensemble experiment (CESM1-LE) and V2 being configured with low- and high-top atmospheric components. The assessment shows CESM2 underestimates snow depth and produces overly uniform snow distributions, whereas CESM1-LE produces a highly variable, excessively-thick snow cover. Observations indicate that snow in CESM2 accumulates too slowly in autumn, too quickly in winter-spring, and melts too soon and rapidly in late spring. The 1950–2050 trends in annual mean snow depths are markedly smaller in CESM2 (−0.8 cm decade^{-1}) than in CESM1-LE (−3.6 cm decade^{-1}) due to CESM2 having less snow overall. A perennial, thick sea-ice cover, cool summers, and excessive summer snowfall facilitate a thicker, longer-lasting snow cover in CESM1-LE. Under the SSP5-8.5 forcing scenario, CESM2 shows that, compared to present-day, snow on Arctic sea ice will: (1) undergo enhanced, earlier spring melt, (2) accumulate less in summer-autumn, (3) sublimate more, and (4) facilitate marginally more snow-ice formation. CESM2 also reveals that summers with snow-free ice can occur ∼30–60 years before an ice-free central Arctic, which may promote faster sea-ice melt.

Plain Language Summary Snow on Arctic sea ice is important for several reasons: it creates a habitat for micro-organisms and mammals, it changes sea-ice growth and melt, and it affects the speed at which ships and people can travel through sea ice. Therefore, investigating how snow on Arctic sea ice may change in a warming climate is useful for anticipating its potential effects on ecosystems, sea ice, and socioeconomic activities. Here, we use experiments from two versions of the Community Earth System Model (CESM) to study how snow conditions change over time. Comparison with observations indicates that CESM2 produces an overly thin, overly uniform snow distribution, while CESM1-LE produces a variable, excessively-thick snow cover. The 1950–2050 snow depth trend in CESM2 is 75% smaller than in CESM1-LE due to CESM2 having less snow. In CESM1-LE, long-lasting, thick sea ice, cool summers, and excessive summer snowfall facilitate a thicker, longer-lasting snow cover. In a warming climate, CESM2 shows that snow on Arctic sea ice will: (1) have greater, earlier spring melt, (2) accumulate less in summer-autumn, (3) sublimate more, and (4) cause marginally more snow-ice formation. CESM2 reveals that snow-free summers can occur ∼30–60 years before an ice-free central Arctic, which may promote faster sea-ice melt.

1. Introduction

Snow is an integral part of the Arctic sea-ice and climate systems, having both positive and negative effects on sea-ice mass balance (Sturm & Massom, 2017; Webster et al., 2018). Snow's reflectivity is important for maintaining a high surface albedo on sea ice during spring and summer (Holland & Landrum, 2015; Perovich et al., 2002; Perovich and Polashenski, 2012), which can delay sea-ice surface melt and melt pond formation (Petrich et al., 2012; Perovich et al., 2017b; Webster et al., 2015). During sea-ice formation, snow is an effective insulator that limits ocean heat flux through sea ice to the atmosphere, thereby hindering sea-ice growth (Maykut, 1978; Sturm et al., 2002). In some cases, a deep snowpack is sufficiently heavy to depress the sea-ice surface into the ocean, allowing seawater to flood the snow and freeze (Provost et al., 2017). With respect to a projected warming of Arctic climate, questions arise as to how snow processes and conditions

will be affected, and whether these changes will fundamentally change the role of snow in the Arctic sea-ice system.

Earth system models are valuable tools for understanding how the snow-ice system may respond to a changing climate. Earlier modeling efforts (Blanchard-Wrigglesworth et al., 2015; Hezel et al., 2012) have projected a decline in snow thickness on Arctic sea ice owing to later sea-ice formation in autumn, an increasing ratio of liquid-to-solid precipitation, and a transition from a perennial to seasonal sea-ice cover. In the western Arctic, these projections have been corroborated by observations showing a decrease in spring snow related to later sea-ice formation in autumn (Webster et al., 2014). Although models show a projected increase in snowfall during winter, which could facilitate a thicker snow cover, the models show a decline in the annual mean snowfall as the Arctic transitions to a rain-dominated summer and autumn (Bintanja & Andry, 2017; Holland et al., 2007; Lique et al., 2016). Such changes in precipitation and the concomitant changes in sea-ice conditions will affect whether snow has a net positive or negative effect on sea-ice mass balance by governing which snow processes dominate. As an example, increased snowfall over thin sea ice may lead to more widespread snow-ice formation, which would act as a negative feedback in sea-ice mass balance.

In this study, we investigate the changes in snow's role in the Arctic sea-ice system under anthropogenic warming using ensemble simulations from two versions of the Community Earth System Model (CESM). For the first time, projections of snow-on-sea-ice processes are quantified and related to changes in sea-ice conditions and precipitation in an Earth system model. Snow thickness distributions are evaluated on temporal and spatial perspectives, and assessed using a synthesis of in situ, airborne, and satellite data. The main findings of our analyses provide new information on the rate of change in snow conditions on sea ice across Arctic basins, which snow processes dominate in different climate states, and the atmospheric and sea-ice conditions that may modify snow's role in the changing Arctic sea-ice system.

2. Data and Methods

The primary data sets of the analysis are freely available CESM output, supplemented by field, airborne, and satellite observations of snow and freeboard conditions. All snow depths referred to hereafter are the geometric snow depth, not the liquid water equivalent snow depth.

2.1. CESM1-LE and CESM2

We analyzed CESM output from multiple model experiments to understand projections of snow conditions on sea ice in a warming climate. We evaluated ensemble simulations from three CESM configurations: (1) CESM Version 1 with the CAM5 atmospheric component (Hurrell et al., 2013) performed as part of the CESM1 Large Ensemble (CESM1-LE) Project (Kay et al., 2015), and CESM Version 2 (Danabasoglu et al., 2020) with the (2) CAM6 atmospheric component, and (3) WACCM6 (Gettelman et al., 2019) atmospheric component. To briefly summarize, the major differences between the CAM6 and WACCM6 atmospheric models are the location of the model top (at 40 km in CAM6 and 140 km in WACCM6) and the presence of prognostic chemistry in WACCM6. The CAM6 and WACCM6 use the same physics and nominal 1° horizontal resolution. For more details on the differences between atmospheric components, we refer readers to Danabasoglu et al. (2020) and Gettelman et al. (2019). The standard CESM2-CAM6 run time is ~4,000 core-hours per model year and gives ~24 model years per real day, while CESM2-WACCM6 is ~30,000 core-hours per model year and gives ~5 model years per real day.

The sea ice component in CESM2 uses the Los Alamos Sea Ice Model (CICE5; Hunke et al., 2015). This is a dynamic-thermodynamic model which utilizes the elastic-viscous-plastic dynamics (Hunke & Dukowicz, 2002) and incorporates a sub-grid-scale ice thickness distribution. Relative to CESM1-LE, which used the earlier CICE4 model version (Hunke & Lipscomb, 2008) with some updates (Holland et al., 2012), the new CICE5 model simulates sea ice as a mushy layer and incorporates prognostic salinity (Bailey et al., 2020; Hunke et al., 2015; Turner et al., 2013). The melt pond formulation is also updated to better reflect differences in ponding on level ice (Hunke et al., 2013). Due to cloud differences between models, Arctic sea ice in CESM2-CAM6 is significantly thinner than in CESM2-WACCM6, which leads to lower summer ice area in CESM2-CAM6 (DeRepentigny et al., 2020; DuVivier et al. 2020). CESM1-LE well captures the Arctic sea

Table 1
The Number of Ensemble Members from Each Model Configuration Used in the Analysis

	Historical	SSP1-2.6	SSP2-4.5	SSP3-7.0	SSP5-8.5	RCP 8.5
CESM1-LE	30	-	-	-	-	30
CESM2-CAM6	11	3	3	3	3	-
CESM2-WACCM6	3	1	5	3	5	-

Note. For the SSP3-7.0 experiment using CESM2-WACCM6, model ensemble members 2 and 3 stop in year 2055.

Abbreviation: CESM, Community Earth System Model.

ice historical state and trends in concentration and thickness (Barnhart et al., 2015; Jahn et al., 2016; Labe et al., 2018).

For CESM1-LE, we analyze output for the 1920–2100 period. Each model configuration and experiment had a different number of ensemble members available (Table 1), which should be considered when interpreting the results, with particular regard to the spread (standard deviation) of the ensemble members. The long-term changes in snow conditions were analyzed primarily using results from the RCP8.5 forcing scenario (van Vuuren et al., 2011) for CESM1-LE and the SSP5-8.5 forcing scenario (O'Neill et al., 2016) for CESM2. These scenarios are designed to achieve the same radiative forcing by the end of the 21st century. However, the transient nature of individual external forcings, including greenhouse gas concentrations and land use change, differs between them as discussed further in O'Neill et al. (2016). Leading up to 2050, which is the primary period used in our analysis, the differences in the individual external forcing terms are quite small. Note that CESM2 SSP5-8.5 simulations reach a higher global mean temperature by 2100 compared to CESM1-LE with RCP8.5 (Meehl et al., 2020), with consequences for Arctic sea ice loss (DeRepentigny et al., 2020). This is likely in part a consequence of the higher equilibrium climate sensitivity in CESM2 (Bacmeister et al., 2020), although differences in the specifics of the forcing scenarios may also play some role.

Using CESM2 output, we evaluate the projections of snow on Arctic sea ice under four different forcing scenarios: SSP1-2.6, SSP2-4.5, SSP3-7.0, and SSP5-8.5. They can be summarized as scenarios with low, medium, medium-to-high, and high radiative forcing conditions and differing shared socioeconomic pathways. Details about these scenarios can be found in O'Neill et al. (2016).

Snow depth on sea ice is analyzed in model grid cells where the sea ice concentration is 15% and greater. In the trend analyses, all values reported have 99% statistical significance. For determining the duration of the snow cover, grid cells with at least 0.01 m of snow and 15% sea ice concentration are counted. We define the duration as the number of days that meet these criteria, regardless of temporal continuity. To explore the relationship between snow-free and ice-free conditions, we compare dates at which these conditions occur in the 80ºN–90ºN region of the central Arctic. We define ice-free conditions as less than one million km^2 in sea ice area and snow-free conditions as a monthly mean snow depth value of 0.01 m or less.

We evaluate five snow processes that constitute the snow mass budget: (1) mass gain from snowfall, (2) mass gain and loss from condensation and sublimation, respectively, (3) mass loss from snowmelt, (4) mass loss from snow-ice formation, and (5) mass change from sea-ice dynamics, which is treated as a residual term in the snow mass budget. The total snow mass is calculated as the difference between the first and last day's snow depth of a given month, converted to units of cm day^{-1} using a constant snow density. A spatial mask of 80ºN–90ºN is applied to mitigate the effects of sea-ice loss on the snow mass budget terms. The 80ºN–90ºN region also isolates the same set of model grid cells where sea ice is predominantly present across model ensemble members and decades for each month. In this way, we are able to evaluate changes in snow processes due to feedbacks within the Arctic system (e.g., less snowfall), rather than have the decreasingly extensive sea-ice cover imprinted on any diagnosed snow trends.

2.2. Field, Airborne, and Satellite Data

Four observational data sets are used to assess the temporal and spatial aspects of snow depth on Arctic sea ice from CESM1-LE and CESM2 (Table 2). These include ground, buoy, airborne, and satellite data.

2.2.1. Field Observations

For examining the seasonal cycle of snow, we co-located and compared monthly snow depths with those measured in situ at the North Pole drifting ice stations in 1954–1991 (Radionov et al., 1997) and derived from drifting ice mass balance (IMB) buoys in 1997–2017 (Perovich et al., 2017a). The drifting ice stations encompassed the central and eastern Arctic, whereas the IMBs were mostly located in the central and western Arctic (Figure S1). The two data sets span historical and contemporary sea-ice conditions, although

Table 2
The Temporal and Spatial Information of Each "Observational" Data Set Analyzed in the Analysis

	Temporal coverage	Temporal resolution	Spatial resolution
North Pole Ice Stations	1954–1991	Every 10 days	10 m
Ice Mass Balance Buoys	1997–2017	Daily	Point measurement
Operation IceBridge	2009–2017	Every spring	40 m
ICESat-2/CryoSat-2	2018–2019	Monthly	25 km

we note earlier work showed no statistical difference in snow accumulation rates between the station and 1993–2013 IMB data (Webster et al., 2014). Similarly, we find no statistical difference between the 1954–1991 and 1997–2017 snow accumulation rates with the exception of August, when greater snow melt was observed in the 1954–1991 data set. A total of 64 IMBs from 1997 to 2017 are analyzed, yielding an average of 1,369 individual recordings per month, a minimum of 907 in February, and a maximum of 1,654 in October. We omit comparisons with the ice station data in summer due to ground measurements ceasing when snow covered less than 50% of the survey lines or when average snow depths were less than 5 cm in thickness (Radionov et al., 1997; Warren et al., 1999), which would create a high bias in the summer station snow depth data.

2.2.2. Airborne Data

We assess the spatial distribution of modeled snow depths for March-April using airborne data. Snow thickness is derived from measurements from the University of Kansas' ultra-wideband microwave radar on NASA's Operation IceBridge mission (Koenig et al., 2010; Kwok et al., 2011; Panzer et al., 2010). The spatial assessment using airborne data is limited to western longitudes due to absence of airborne surveys in the eastern Arctic. We compare averages between the modeled and observed snow depths in grid cells where at least 100 airborne measurements were collected. The airborne data do not include snow-free surfaces and therefore may be biased high. Another source of bias may be the effects of saline snow, which can cause a shallower detection of the assumed snow-ice interface and thus underestimate snow depth (Nandan et al., 2017).

2.2.3. Satellite Data

Due to the limitation of ground and airborne observations both in space (i.e., western Arctic) and time (spring season), we use data from NASA's Ice, Cloud, and land Elevation Satellite 2 (ICESat-2) and ESA's CryoSat-2 missions to examine snow depth distributions for October 2018–April 2019 across the entire Arctic basin. ICESat-2's laser altimeter theoretically detects the surface of the snow-covered (or snow-free) sea ice, and, using a reference sea level height and assumed snow density, total freeboard is determined (Kwok et al., 2019). CryoSat-2 theoretically detects the snow-ice interface and, using a sea level reference, the sea-ice freeboard is derived (Kwok & Cunningham, 2015). The difference between the total (snow and ice) freeboard and sea-ice freeboard yields snow depth (Figure 1) (Kwok et al., 2020). The inferred snow depth from the freeboard differences has several issues that warrant consideration: (1) the spatio-temporal sampling between ICESat-2 and CryoSat-2 is not consistent due to their differing orbits for 2018–2019, (2) CryoSat-2 sea-ice freeboards may be overestimated due to an erroneously shallow detection of an interface within the snowpack resulting from the presence of brine (Nandan et al., 2017), flooding (Provost et al., 2017) or other structural complexities within the snowpack, and (3) possible sub-surface scattering of ICESat-2 photons, leading to a low bias in total freeboard. The combined effect of biases in (2) and (3) may lead to an underestimation of inferred snow depth. Accordingly, the inferred snow depths may
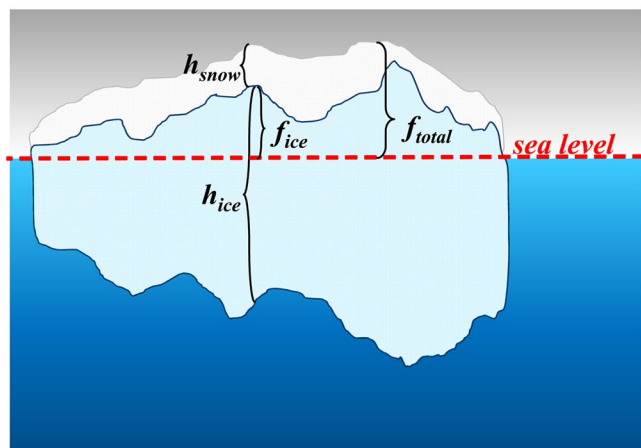

Figure 1. A schematic showing the relationship between snow depth, sea ice freeboard, sea ice thickness, and total (snow and sea ice) freeboard as shown in Equation 1.
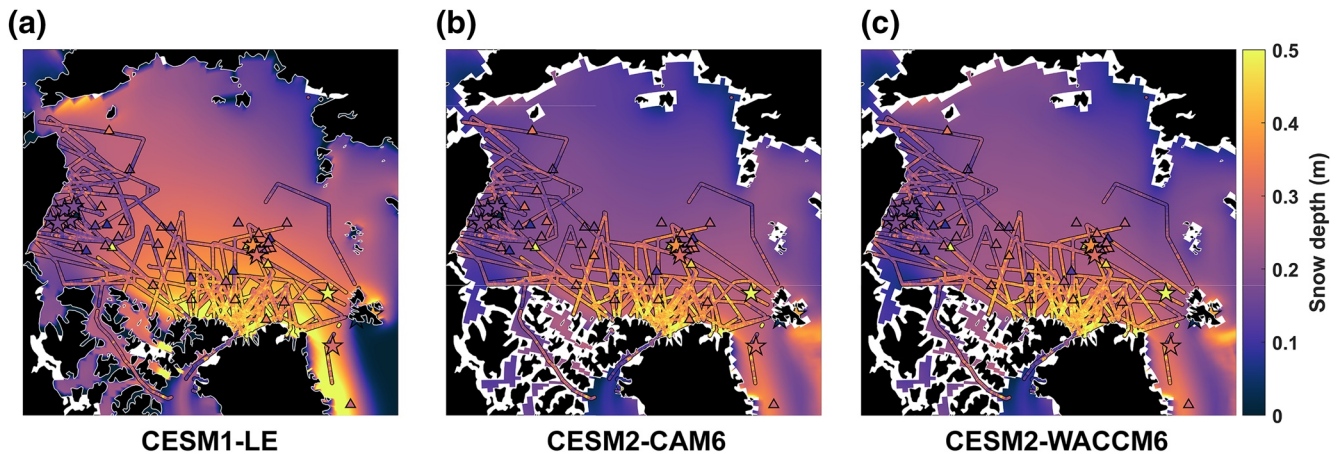
Figure 2. The 2000–2017 modeled spring (March-April) snow depth distributions with ground, buoy, and airborne observations overlaid from the 2000–2017 period. The stars represent snow depth data from field camps while the triangles are those from drifting IMB buoys. The model results are from: (a) CESM1-LE; (b) CESM2-CAM6; and (c) CESM2-WACCM6.

be a reasonable lower bound when comparing with the modeled snow depths. Comparing total freeboard from ICESat-2 with those estimated from CESM variables can serve as an additional assessment of modeled snow depths. Since snow and ice densities, sea ice freeboard, and snow depth values are known from CESM, we can use them to infer total freeboard.

Assuming hydrostatic balance for sea ice, total freeboard (f_t) can be solved for using:

$$f_t = h_s \frac{\rho_w - \rho_s}{\rho_w} + h_i \frac{\rho_w - \rho_i}{\rho_w}, \tag{1}$$

where h_s is the snow depth, h_i is the sea ice thickness, ρ_w is the density of seawater, ρ_s is the density of snow, and ρ_i is the density of sea ice. Density values of snow and sea ice—330 kg m^{-3} and 917 kg m^{-3}, respectively—are fixed in the model. Seawater density is not held constant in CESM; however, we assumed a seawater density of 1,026 kg m^{-3} for our calculations, which is a commonly used value in the altimetry community (e.g., Kwok et al., 2020). We compared inferred snow depths from ICESat-2 and CryoSat-2 freeboards (Kwok et al., 2020) with those directly available from CESM to investigate possible seasonal and regional biases in snow depth distributions. We use monthly means of CESM variables for 2018–2019 from all ensemble members for the snow depth comparisons and to infer total freeboard. The 2018–2019 period was chosen due to the temporal overlap with ICESat-2 data; however, we note different sea-ice extents between the model and passive microwave observations (Fetterer et al., 2017) (Figure S2).

3. Results and Discussion

We first present the spatial and temporal assessments of simulated snow depths from comparisons with in situ, buoy, airborne, and satellite data in Section 3.1. Section 3.2 describes the long-term changes in snow depth under different forcing scenarios for CESM1-LE and CESM2 and the changes in the seasonal cycle of snow in relation to sea-ice conditions. Section 3.3 presents the decadal changes in the snow mass budget, how the budgets differ between models, and the general spatial distribution of snow processes over time.

3.1. Comparison With Observations

3.1.1. Spatial Distribution

The modeled snow depths for the spring season exhibit a similar spatial pattern of Arctic snow across all model configurations: deep snow is found north of Greenland and the Canadian Archipelago and thinner snow is predominantly located in the peripheral seas (Figure 2). An exception to this pattern is the exceptionally deep snow (i.e., greater than 1 m in depth) directly east of Greenland in CESM1-LE. Qualitatively,
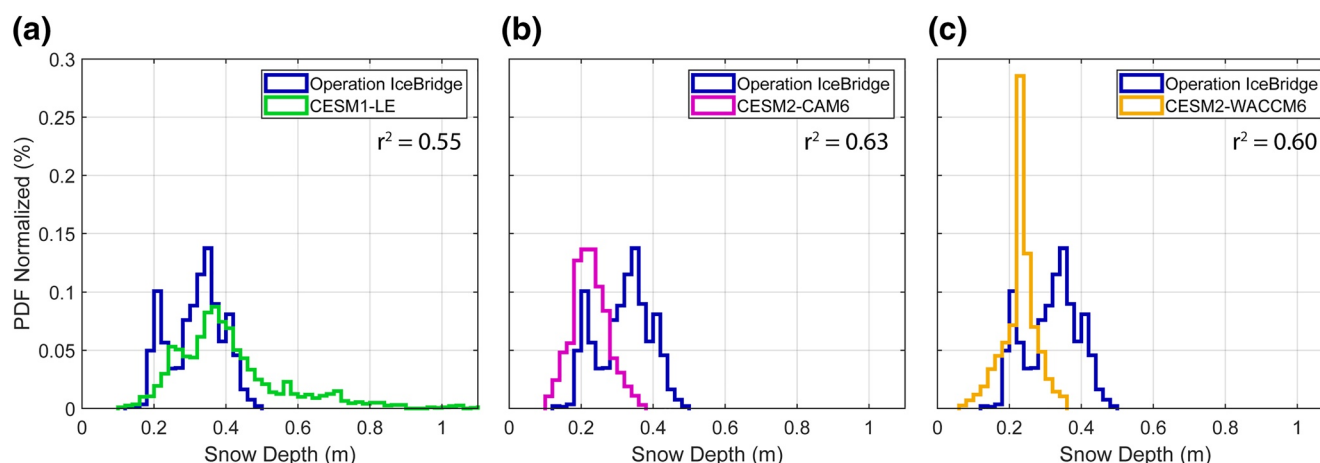
Figure 3. A comparison of the 2009–2017 spring (March-April) snow depth distributions between Operation IceBridge and model data. (a) snow depth distributions retrieved by airborne radar compared to those simulated by CESM1-LE; (b) the same as in (a) comparing radar retrievals and CESM2-CAM6 snow depth distributions; and (c) the same as (a) comparing radar retrievals and CESM2-WACCM6 snow depth distributions. Correlation coefficients were statistically significant at the 99% level. The bin width is 2 cm.

the cross-basin distribution of snow is consistent with ground and airborne observations; however, the range in snow depth differs. Snow depths in CESM1-LE were thicker and distributed more heterogeneously than the airborne observations, with snow depths being greater than 1 meter in places (Figure 3). CESM1-LE exhibited a weak bimodal snow depth distribution that is qualitatively similar to that in the Operation IceBridge retrievals. The timing of sea-ice freeze-up and age of sea ice create this bimodal distribution; 1-year sea ice has less time to accumulate snow and therefore tends to have thinner snow conditions than multiyear sea ice in the Lincoln, Beaufort, and Chukchi seas (Kurtz & Farrell, 2011; Webster et al., 2014). The bimodal distribution is not captured at all in CESM2, and snow depths in both CAM6 and WACCM6 are thinner and more uniform than the airborne observations and CESM1-LE. The largest discrepancy occurs north of Greenland (i.e., Lincoln Sea region), where CESM2 snow depths are ~10–20 cm thinner than the airborne observations. Interestingly, CESM2-WACCM6 has a more uniform snow depth distribution than CESM2-CAM6, despite having greater variability and a larger range in sea ice thickness along the Operation IceBridge surveys (Figure S3).

3.1.2. Seasonal Cycle

Comparisons of CESM2 snow depths with in situ, buoy, and satellite data (Figures 4 and 5) suggest three important findings for the simulated seasonal cycle. CESM2-CAM6 and CESM2-WACCM6 appear to: (1) underestimate snow accumulation and depth in autumn, (2) overestimate the rate of increase in snow depth between late winter and early spring, and (3) melt snow too early and too rapidly from late spring into early summer. For CESM1-LE, the results were in mixed agreement with the observations.

In Situ and Buoy Comparisons:

We begin with the CESM2 analysis at the onset of the snow accumulation season in August, when snow depths increase from their minimum values (Figure 4). Note that the ice station (1954–1991) and IMB (1997–2017) data represent different time periods. In August–November, snow accumulates rapidly at the IMBs and ice stations, with IMBs having slightly larger accumulation rates. The buildup of the snowpack in CESM2-CAM6 and CESM2-WACCM6 was approximately half (~2 cm month^{-1}) the rate recorded by the IMBs (~5 cm month^{-1}) and at the drifting ice stations (~4 cm month^{-1}). From January to May, the rate of change in CESM2 snow depth is larger (~3 cm month^{-1}) than both the IMBs, which decreases by ~ −1 cm month^{-1}, and the ice stations (~2 cm month^{-1}), despite CESM2 snow depths being thinner than the observations.

During the early melt season, the observations and models exhibit disparate snowmelt onset dates and rates. In CESM2, a dramatic decline in snow depth began in May, while the snowmelt rates recorded by the IMBs and at the ice stations were most extreme in June. CESM2 exhibited snow-free conditions earlier
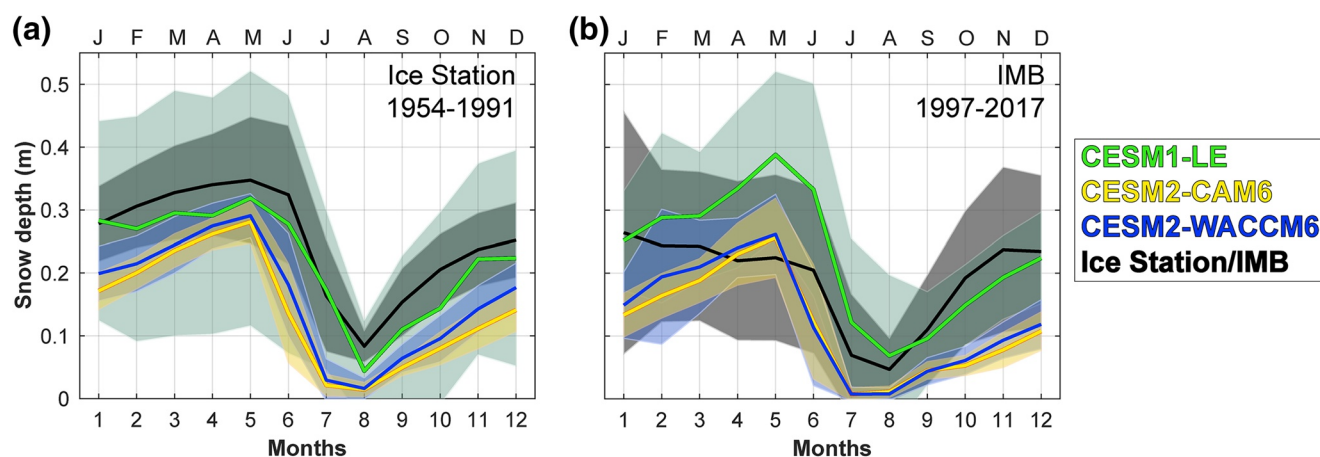
Figure 4. The mean (solid) and standard deviation (shaded spread) in snow depth for the (a) drifting ice stations and CESM configurations, and (b) IMBs and CESM configurations for each month at all drifting IMB/ice station locations. The squared correlation coefficients with the ice stations were 0.15, 0.50, and 0.53 for CESM1-LE, CESM2-CAM6, and CESM2-WACCM6, respectively. The squared correlation coefficients with the IMBs were 0.09, 0.12, and 0.12 for CESM1-LE, CESM2-CAM6, and CESM2-WACCM6, respectively.

than the IMBs (July vs. August), which has important implications for a positive albedo feedback. CESM2 snow depths were thinner than the drifting ice station data, but produce a representative seasonal cycle for the 1954–1991 period. In contrast, the modeled seasonal cycle of the 1997–2017 period has poor agreement with the IMB data, although this relationship likely worsens due to the large heterogeneity in point IMB measurements relative to mean values of model grid cells and ground survey lines.

CESM1-LE snow depths had considerably larger variability at the IMB and ice station locations than CESM2 (Figure 4), which should be considered when interpreting the following results. The autumn accumulation rates in CESM1-LE compares well with the ice station and IMB observations. From January to May, snow accumulation rates diverge between the 1954–1991 and 1997–2017 periods. Both CESM1-LE and ice station accumulation rates were ~1–2 cm month^{-1}, whereas CESM1-LE rates during the contemporary period were ~3 cm month^{-1} and the IMB observations were −1 cm month^{-1}. In summer, both CESM1-LE and the ice stations showed the same melt rate of -9 cm month^{-1}. At the IMB sites, the melt rate in CESM1-LE was nearly double the IMB observations (~−11 cm vs. −6 cm month^{-1}). In summary, CESM1-LE has good agreement with the observations relative to CESM2, better simulates the historic seasonal cycle, but poorly captures the seasonal cycle for the contemporary period.

Satellite Comparison

To assess snow depth distributions across the entire Arctic basin, we compared modeled snow depths with inferred snow depths from ICESat-2 and CryoSat-2 freeboard data (Figure 5). Such a comparison gives greater insight into the unique geographic differences of snow conditions between Arctic regions. The results shown in Figure 5 are from CESM2-WACCM6 and comparable to those from CESM2-CAM6 (Figure S4).

During the buildup of the snowpack in October, CESM2-WACCM6 underestimates snow depth by −8% relative to the inferred snow depths. In multiyear ice areas immediately north of the Canadian Archipelago, CESM2-WACCM6 snow depths and total freeboards remain smaller than the those derived from satellite data throughout October-April (Figures 5 and S5). From November onward, snow in the central Arctic basin, southern Laptev Sea, and northern Kara and Barents seas deepens more rapidly in CESM2-WAC-CM6 than that derived from satellite data. By April, the Arctic average snow depth is ~18% thicker in CESM2-WAACCM6 than that derived from satellite data, but there are regional exceptions, such as in the northern Chukchi Sea and north of the Canadian Archipelago.

The results in Figures 5 and S6 show strong spatial heterogeneity between Arctic regions, as well as the inter-annual variability in atmosphere-snow-ice conditions imprinted on the ICESat-2 data. For example, the feature in the northern Chukchi Sea in March and April has an inferred snow depth ~10–20 cm deeper than that in CESM2-WACCM6. The source of this feature is the locally large, total freeboard values in ICESat-2
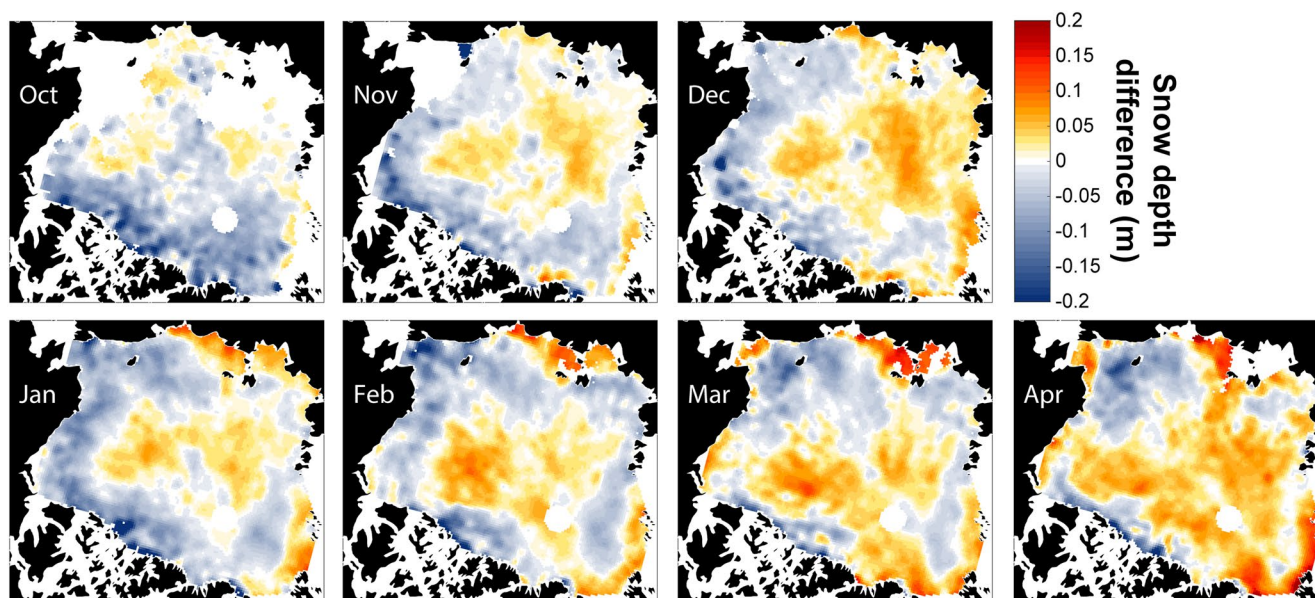
Figure 5. The difference in snow depth directly available from CESM2-WACCM6 minus that derived from ICESat-2 and CryoSat-2 data. The CESM2-WACCM6 data and ICESat-2/CryoSat-2 data cover 2018–2019. From 88ºN to 90ºN is a gap in ICESat-2 coverage due to the satellite orbit. Consequently, no data are available, and a white pole hole is present in all panels.

data. In Kwok et al. (2020), the feature was attributed to deep snow from anomalously high cyclone activity and cyclone-associated snowfall over sea ice in the northern Chukchi Sea during the 2018–2019 snow accumulation season relative to the 1979–2019 cyclone climatology (Webster et al., 2019).

3.2. Long-Term Changes

3.2.1. Coverage

Snow depth on Arctic sea ice declines under all forcing scenarios over 1850–2100 in CESM2-CAM6 and CESM2-WACCM6 (Figure 6). Prior to 1950, the trend in mean annual snow depth remains relatively unchanged. From 1950 to 2050, all scenarios have similar projections, ranging from -0.6 cm per decade (SSP3-7.0) to −0.8 cm per decade (SSP5-8.5). For 2050–2100, the decline in annual mean snow depth strongly corresponds to the forcing scenarios, with the deepest snow cover occurring under the weakest forcing
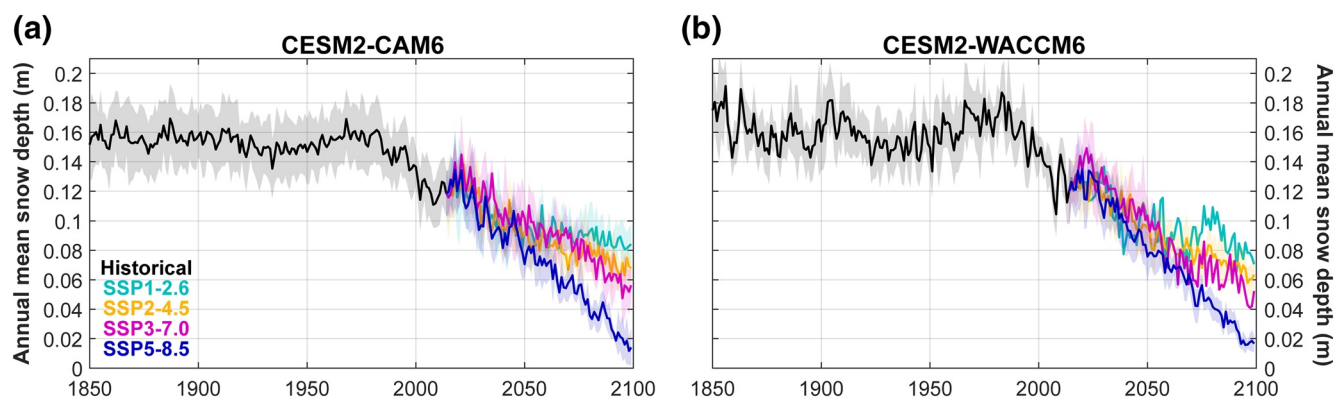

Figure 6. Projections of annual mean snow depth over 80ºN–90ºN under different forcing scenarios for (a) CESM2-CAM6 and (b) CESM2-WACCM6. The historical period refers to simulations of 1850–2015. The solid lines represent the model ensemble mean, while the spread is the standard deviation among ensemble members. Please note that the spread, or lack thereof, is largely due to the number of available ensemble members (see Table 1).
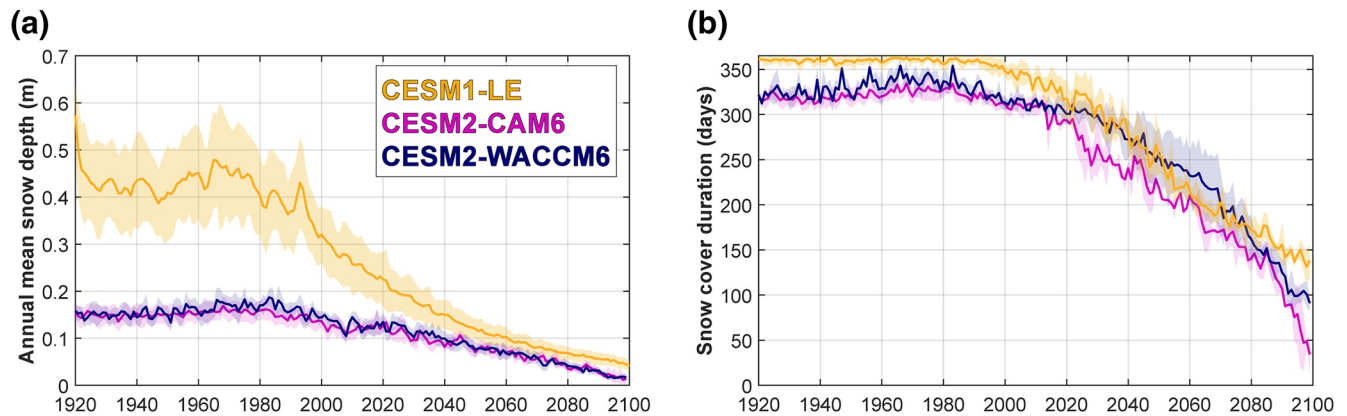
Figure 7. (a) The annual mean snow depth at 80ºN–90ºN for historical models runs and projected under the SSP5-8.5 and RCP8.5 forcing scenario for CESM2 and CESM1-LE, respectively; and (b) the number of days (duration) with at least 0.01 m snow depth and 15% sea ice concentration over 80–90ºN for historical models runs and projected under the SSP5-8.5/RCP8.5 forcing scenario. The spread in both panels is the standard deviation across model ensemble members, while the solid line is the ensemble mean. Note, the number of ensemble members changed from 11 to two for CESM2-CAM6 and 3 to 5 for CESM2-WACCM6 in 2015, which affects the spread.

scenario (SSP1-2.6; −0.2 to −0.3 cm decade^{-1}) and the thinnest snow cover occurring under the strongest forcing scenarios (SSP5-8.5; −1.3 to −1.4 cm decade^{-1}).

As evidenced in Figure 2, snow conditions between CESM1-LE and CESM2 are strikingly different. The annual mean snow depth in CESM1-LE (for 80ºN–90ºN) is approximately twice as thick as that in CESM2-CAM6 and CESM2-WACCM6 for the 1920–2100 period (Figure 7a). The trends over 1950–2050 also show marked differences between model configurations. The annual mean in snow depth declines at −3.6 cm decade^{-1} in CESM1-LE, whereas the trends in CESM2-CAM6 and CESM2-WACCM6 are notably more gradual at −0.8 cm decade^{-1}. The observed trend, which is limited to the 1954–2013 March–April season only, was −2.9 cm decade^{-1} (Webster et al., 2014). We find that the 1954–2013 March–April trend in CESM1-LE (−3.0 cm decade^{-1}) shows strong agreement with the observed trend, while trends in CESM2 are considerably smaller (−0.5 to −0.7 cm decade^{-1}). The discrepancy in trends between model versions may be partly explained by the thinner snow depth conditions in CESM2 for the earlier part of its simulated record (Figure 7a).

The snow cover in CESM1-LE was more persistent throughout the 1920–2100 period than that in CESM2 (Figures 7b and 8). We attribute this in part to the greater coverage and persistence of sea ice (DeRe-
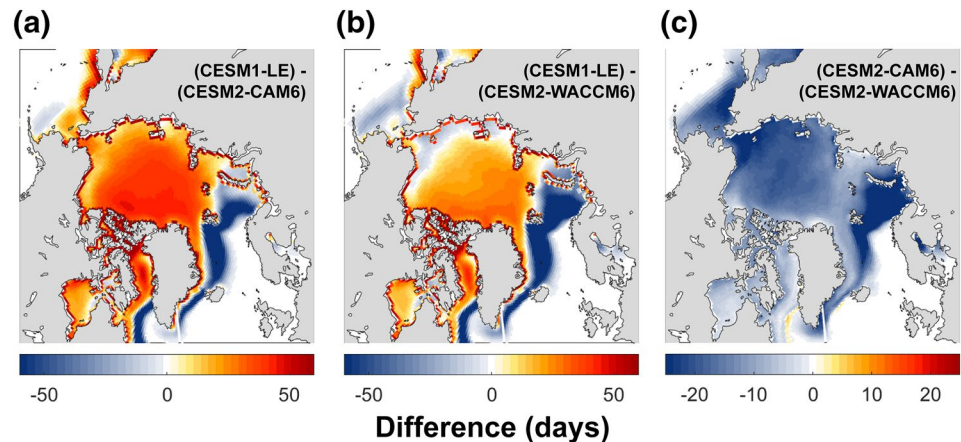

Figure 8. The difference in the snow cover duration, defined as the number of days when the snow cover was at least 0.01 m thick and sea ice concentration at least 15%, over 1920–2100 for (a) CESM1-LE minus CESM2-CAM6, (b) CESM1-LE minus CESM2-WACCM6, and (c) CESM2-CAM6 minus CESM2-WACCM6.
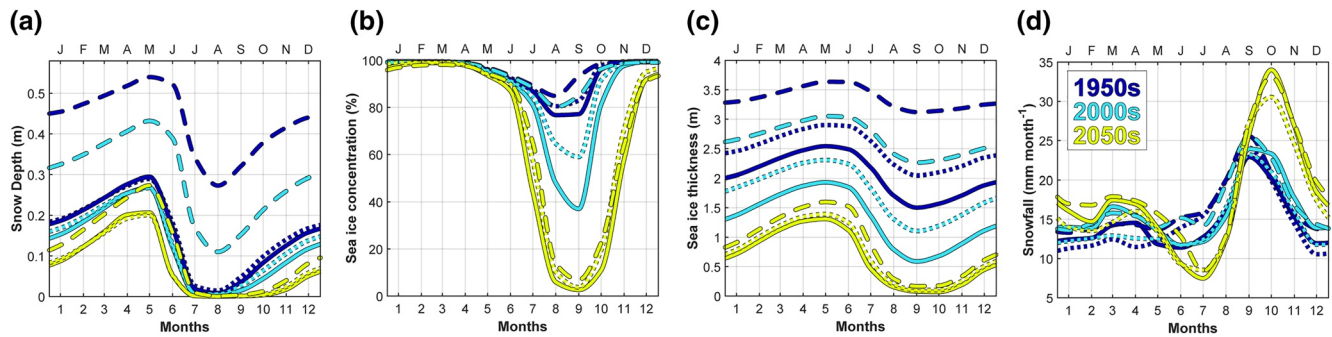
Figure 9. Decadal averages of (a) snow depth, (b) sea ice concentration, (c) sea ice thickness, and (d) snowfall over 80ºN–90ºN for the 1950s, 2000s, and 2050s from CESM1-LE (dashed), CESM2-CAM6 (solid) and CESM2-WACCM6 (dotted) under the RCP8.5 and SSP5-8.5 forcing scenarios.

pentigny et al., 2020) as well as to excessive snowfall and cooler summers in CESM1-LE (McIlhattan et al., 2017, 2020), which helps retain a high surface albedo and consequently promotes a negative albedo feedback (Light et al., 2015). In contrast, Arctic sea ice in CESM2 is less extensive, forms later, and the snowfall rate is lower than in CESM1-LE (DeRepentigny et al., 2020; McIlhattan et al., 2020). When comparing CESM2 atmospheric components, both the snow and sea-ice covers in CESM2-WACCM6 survive longer during the summer melt season than those in CESM2-CAM6 (Figures 7b and S7). As shown in DuVivier et al. (2020a), CESM2-CAM6 has more incoming shortwave radiation, which may promote earlier, faster melt of the snow cover and facilitate a stronger positive albedo feedback. The largest differences in snow cover duration occur in the Kara and Greenland seas (Figure 8), with differences of more than 50 days. As shown in Figures 3 and 5 in DuVivier et al. (2020a), sea ice is considerably thinner and less extensive in CESM2-CAM6 than CESM2-WACCM6 in these seas. North of 75°N, the average difference in snow cover duration was 19 days (34 days) between CESM1-LE and CESM2-WACCM6 (CESM2-CAM6).

3.2.2. Seasonality

Across all CESM configurations, the snow depth minimum occurs in mid-August, nearly a month before the sea ice minimum extent in September (Figure 9a). This suggests that, while new snow may accumulate in mid-summer, the albedo impact is not sufficient to halt summer ice melt and that other factors such as bottom melt sustain summer ice loss through to mid-September. This is further supported by the prolonged decrease in sea ice thickness after the snow depth minimum (Figures 9a and 9c). The snow depth maximum occurs at similar times across all model configurations; however, peak snowmelt is distinctly earlier in CESM2 than CESM1-LE in the 1950 and 2000s. DuVivier et al. (2020a) found that CESM2-
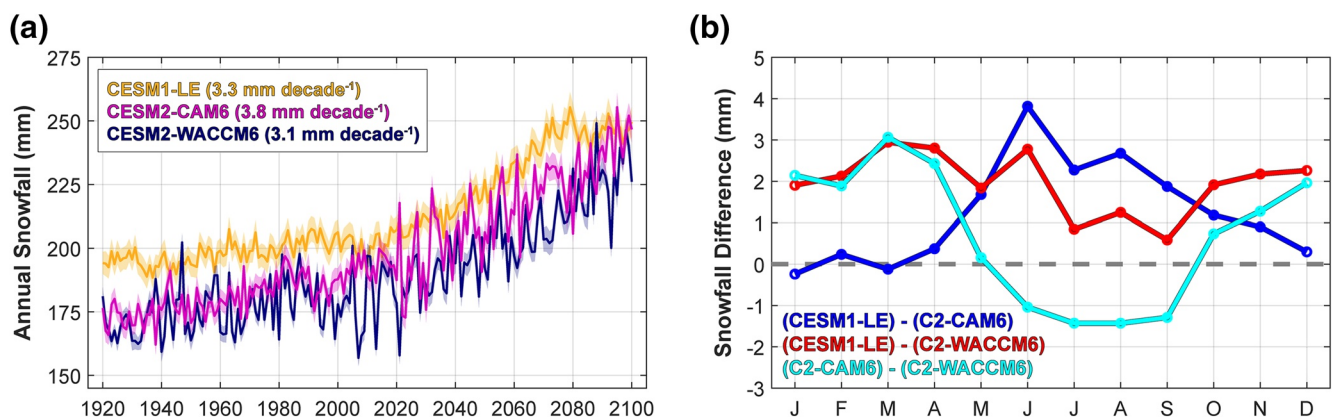

Figure 10. (a) The annual snowfall, in water equivalent, over 80ºN–90ºN for all model configurations from 1920 to 2100 under the RCP 8.5 and SSP5-8.5 forcing scenarios; (b) The difference between model configurations in monthly mean snowfall averaged over 1920–2100 and 80ºN–90ºN under the same forcing scenarios as panel (a).
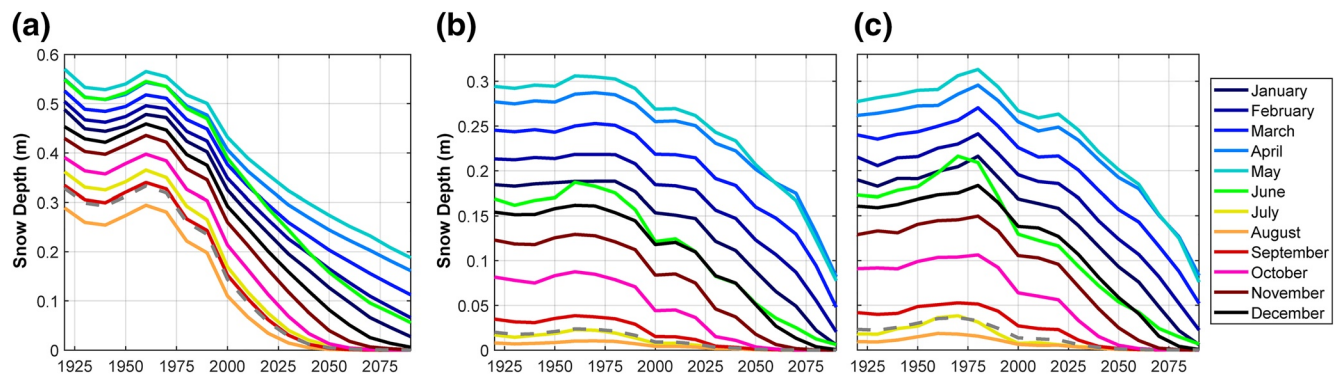
Figure 11. Mean monthly snow depths over 80ºN–90ºN for (a) CESM1-LE (b) CESM2-CAM6, and (c) CESM2-WACCM6 under the RCP8.5 and SSP5-8.5 forcing scenarios. The gray dashed line represents the summer (July, August, and September) average. Note the scale change between panel (a) and panels (b–c) to better illustrate the large snow depths in CESM1-LE.

CAM6 exhibits earlier, stronger melt than CESM2-WACCM6 due to fewer clouds, which subsequently allows greater shortwave radiation at the surface. By the 2050s, peak melt is concurrent across all model configurations.

In general, CESM1-LE produces more annual snowfall than CESM2 over 80ºN–90ºN (Figures 9d and 10a). The largest differences occur in June-August for CESM2-CAM6 ($\sim$2–4 mm month^{-1}) (Figure 10b), when freshly accumulated snow has the largest effect in increasing surface albedo (Holland & Landrum, 2015; Light et al., 2015). Although the 1920–2100 trends in snowfall for CESM1-LE and CESM2-WACCM6 are similar (3.3 and 3.1 mm decade^{-1}, respectively), CESM1-LE has more annual snowfall (+15 mm) at the beginning of the time-series (Figure 10). CESM2-CAM6 also produces less snowfall than CESM1-LE for the earlier part of the time-series; however, its snowfall increases by 3.8 mm decade^{-1} and produces a comparable amount of total snowfall to CESM1-LE by 2100 (Figure 10a). The comparison between CESM2-CAM6 and CESM2-WACCM6 reveals that CESM2-CAM6 has slightly more annual snowfall than CESM2-WAC-CM6 for 1920–2100, averaging 198 versus 189 mm. However, CESM2-WACCM6 has more snowfall than CESM2-CAM6 during the summer melt season of 1.3 mm month^{-1} (Figure 10b).

Snow-free summers (mean snow depth value of 0.01 m or less in 80ºN–90ºN) become an emerging feature in the 1930s for CESM2-CAM6 and 2000s for CESM2-WACCM6, whereas the first snow-free summer occurs in the 2040s in CESM1-LE (Figure 11). In CESM2, thin snow (i.e., less than 3 cm) occurs throughout the historical runs in summer, which may be related to less perennial sea ice in CESM2 relative to CESM1-LE (DeRepentigny et al., 2020), as well as the warmer summer temperatures in CESM2-CAM6 (McIlhattan et al., 2020). In the context of sea-ice retreat, ice-free summers (less than one million km^2 covering 80ºN–90ºN) first occur in the 2020s, 2030s, and 2040s for CESM2-CAM6, CESM2-WACCM6, and CESM1-LE, respectively. These results indicate that while the loss of snow is a reinforcing factor in the positive albedo feedback (Holland & Landrum, 2015), snow-free summers can persist for $\sim$30–60 years before the onset of an ice-free central Arctic in CESM2. In CESM1-LE, the first snow-free and ice-free summers occur within the same decade.

3.3. Snow Processes

Under the SSP5-8.5 forcing scenario, the 1950s to 2050 decadal changes in the snow mass budgets of CESM2-WACCM6 and CESM2-CAM6 reveal: (1) greater, earlier spring melt, (2) less snow accumulation in late summer and early autumn, (3) slightly enhanced winter snow accumulation in CESM2-WACCM6, but less winter accumulation in CESM2-CAM6, (4) less condensation and more sublimation, and (5) a marginal increase in snow-ice formation (Figures 12 and 13).

The largest sink in the snow mass budget is snow melt. Snow melt in spring is more than three times greater in the 2050s than in the 1950s in CESM2-WACCM6, and doubling in the 2050s in CESM2-CAM6 (Figures 12c and 12d). In the 2000 and 2050s, snow melt in July–September decreases due to the absence
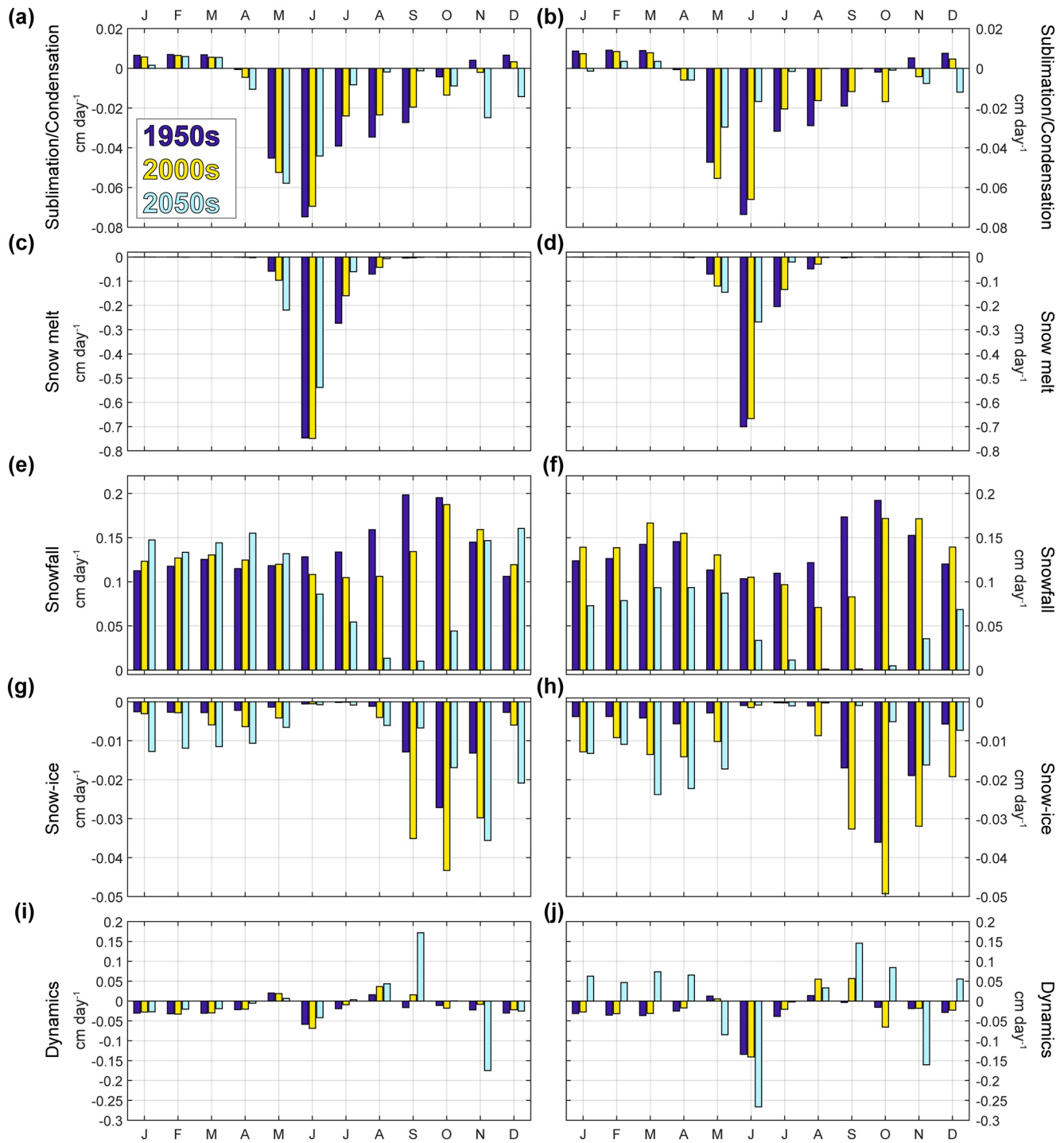
Figure 12. Decadal averages from (left) CESM2-WACCM6 and (right) CESM2-CAM6 of snow processes that constitute the snow mass budget over the annual cycle. Averages are taken over 80ºN–90ºN for the 1950s, 2000s, and 2050s under the SSP5-8.5 forcing scenario. The snow processes include: (a and b) sublimation and condensation, (c and d) snow melt, (e and f) accumulation from snowfall, (g and h) snow-ice formation, and (i and j) dynamics.

of snow and sea ice. August–October snow accumulation rates in CESM2-WACCM6 decreases by ∼88% by the 2050s largely due to sea-ice loss, but increases by ∼31% in December–February. In contrast, snow accumulation in CESM2-CAM6 decreases in all months, with a 64% decrease in the annual total (Figures 12e and 12f), despite the increase in annual snowfall (Figure 10a). Although sublimation and condensation play
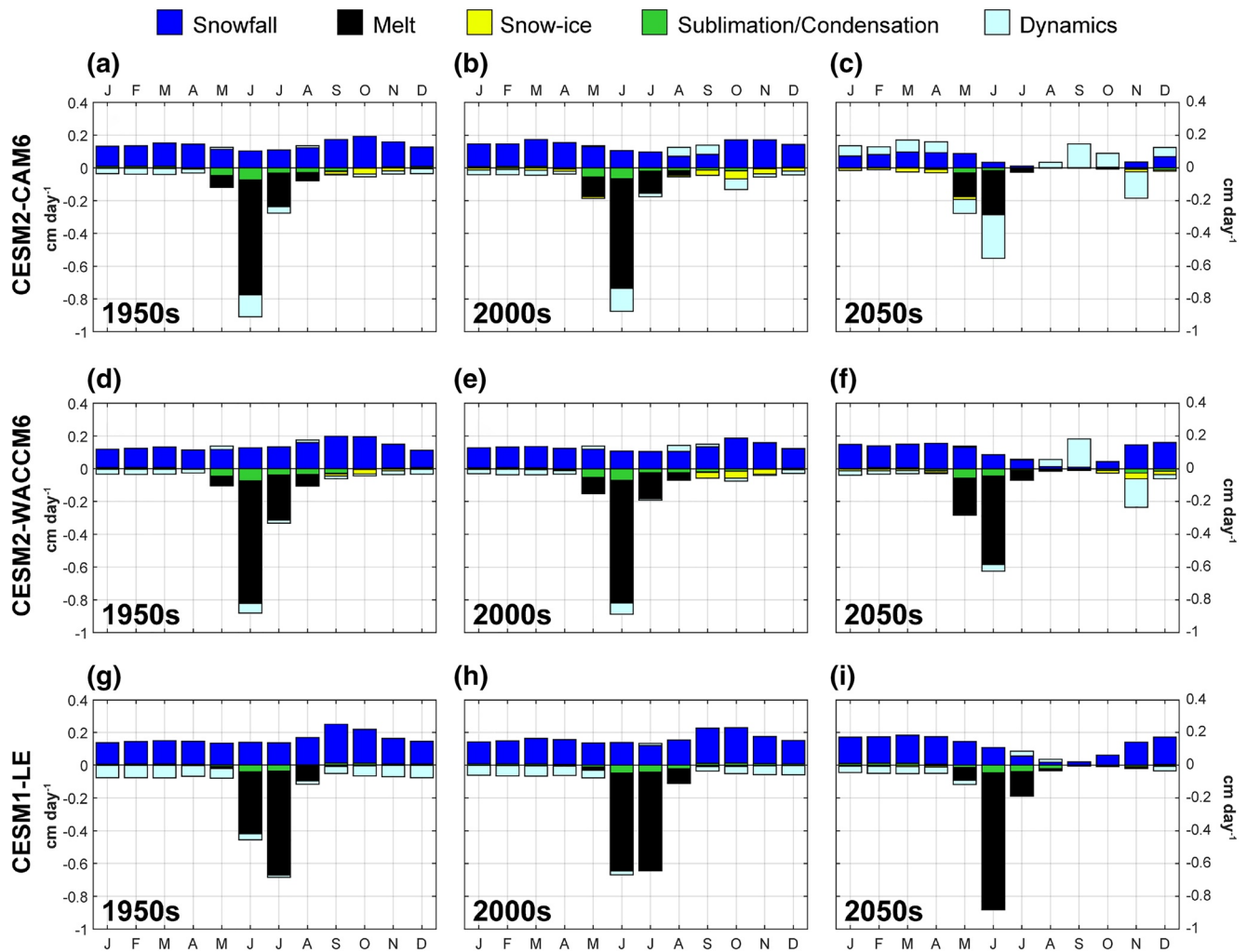
Figure 13. Snow processes that comprise the snow mass budget for (a–c) CESM2-CAM6, (d–f) CESM2-WACCM6, and (g–i) CESM1-LE. The decadal averages for 1950s, 2000s, and 2050s over 80ºN–90ºN are shown.

very small roles in the snow mass budget, we found an overall shift from condensation (positive mass contribution) to sublimation (negative mass contribution) (Figures 12a and 12b) between the 1950 and 2050s.

As sea ice thins and snowfall increases, sea ice may become more susceptible to snow-ice formation if snow accumulation rates are sufficiently large. We found rates of snow-ice formation decrease by ∼0.01–0.03 cm day^{-1} in September–October in both CESM2 model configurations between the 1950 and 2050s (Figures 12g and 12h). We attribute this decrease due to the absence of sea ice, which forms progressively later during the 21st century (Figure 9b). In contrast, snow-ice formation in January–April increases by ∼0.01–0.02 cm day^{-1}, which may correspond with thinner sea ice (Figure 9c) and more snowfall (Figure 10a). Despite the seasonal changes in snow-ice formation rates, its contribution to the snow mass budget remains small in all future decades under the RCP 8.5 and SSP5-8.5 forcing scenarios (Figures 12, 13, and S8). This result indicates that the snow-ice system maintains a sufficiently high ratio of sea ice-to-snow thickness to preclude widespread snow-ice formation in current and future decades in the central Arctic.

Throughout most months and decades, dynamics play a larger role in the snow mass budget than sublimation-condensation and snow-ice formation. Sources of dynamic processes are challenging to disentangle and understand due to the dynamics term being the residual of changes in daily snow depth minus the
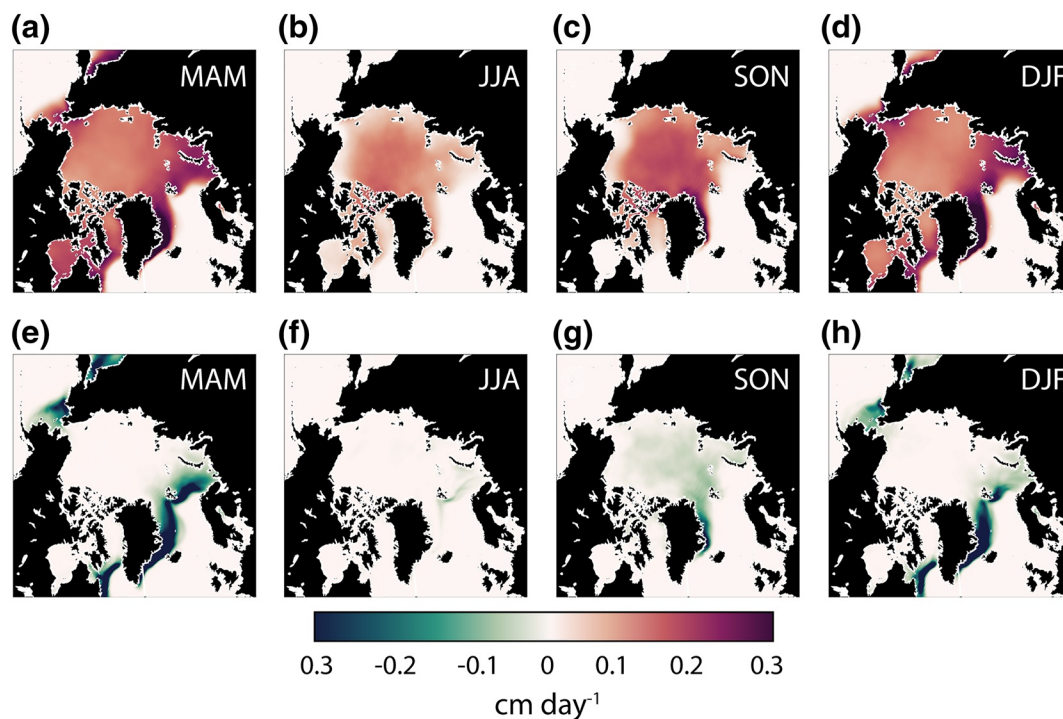
Figure 14. The 2000–2009 average (a–d) snow mass gain from snowfall and (e–h) snow mass loss from snow-ice formation for each season in CESM2-WACCM6.

contribution of other snow mass budget processes. The dynamic changes may result from snow-covered ice being advected into or out of a region, and/or may also come from rafting and ridging, during which 50% of the snow is lost to the ocean (Hunke et al., 2015). Separating and quantifying the effects of ice advection and ridging on the snow mass budget therefore requires a more detailed analysis which may benefit from a Lagrangian framework as in DuVivier et al. (2020).

Regarding the spatial distribution of snow processes, similar patterns emerge between specific snow conditions and atmosphere-snow-ice interactions. In the 2000s, the mass gain from snowfall is largest in the northern Atlantic Ocean and Bering Sea, where the north Atlantic and north Pacific storm tracks intersect with the Arctic (Figures 14a–14d). These areas also coincide with thinner sea ice (see Figure 5 in DuVivier et al., 2020a), early season bottom sea-ice melt (Figure S9), and a greater prevalence of snow loss due to snow-ice formation in CESM2-CAM6 (not shown) and CESM2-WACCM6 (Figures 14e–14h). As future models improve in spatial resolution and treatment of physics, greater understanding can be gleaned of the governing mechanisms from such regional differences in the snow-sea ice system.

4. Conclusions

In this study, we used climate model experiments to investigate how snow conditions on Arctic sea ice may respond to a warming climate. We evaluated Versions one and two of CESM using in situ, airborne, and satellite observations. The assessment shows that CESM2-CAM6 and CESM2-WACCM6 produce a snow cover that is too uniform and too thin, whereas snow in CESM1-LE is heterogeneous and excessively thick. Snow in all model configurations thins in a warming climate; however, the 1950–2050 trend in CESM2 is 75% smaller than that in CESM1-LE owing to thinner snow in CESM2.

The differences in the mean sea-ice state and precipitation are the primary contributing factors to dissimilar snow conditions between model configurations. For example, the combined effect of a perennial, thick sea-ice cover, cool summers, and excessive summer snowfall in CESM1-LE facilitates a thicker, longer-lasting snow cover relative to snow in CESM2. These results highlight the importance of the strong coupling

between snow, sea-ice, and atmospheric conditions (Webster et al., 2018), which manifests in the trends of snow depth under the future forcing scenario between model configurations.

All model configurations show similar seasonal changes in the following snow processes for future projections:

1. Earlier, enhanced snow melt in spring;
2. Less snow accumulation in summer and early autumn;
3. More sublimation year-round; and
4. Slightly more snow-ice formation.

These changes have important implications for climate feedbacks and the sea-ice mass budgets in the Arctic. An earlier spring melt (process 1) would promote a positive albedo feedback and enhance sea-ice melt. Less summer snow accumulation (process 2) would also create a positive albedo feedback; however, since this impacts late summer when solar insolation is low, its influence would be reduced relative to the earlier spring melt. Perhaps more importantly, less snow in autumn as sea ice is beginning to form would allow sea ice to grow faster due to a reduction in the snow's insulating effect. To better understand the net effects of these projected snow changes for the ice mass budgets and climate feedbacks, model experiments with prescribed snow changes would be useful and will be pursued in future work.

It is uncertain what the effects of greater sublimation (process 3) will have on the atmospheric state, but more may be learned from the recent observations from the Multidisciplinary drifting Observatory for the Study of Arctic Climate (MOSAiC) expedition and using such observations to guide accompanying model experiments. While snow-ice formation increases (process 4), it still has a negligible contribution to the total Arctic snow mass budget. However, there may be specific regions where this process becomes increasingly important over time, such as Bering Strait and Fram Strait (Figures 14e–14h). Combined modeling and observational efforts could progress the science and understanding of the atmosphere-snow-ice interactions unique to these (and other) regions, especially in light of testing improved physics and resolutions in ongoing model development.

Data Availability Statement

Computing and data storage resources, including the Cheyenne supercomputer (https://doi.org/10.5065/D6RX99HX), were provided by the Computational and Information Systems Laboratory (CISL) at NCAR. Previous and current CESM versions are freely available at: http://www.cesm.ucar.edu/models/cesm2/. The CESM2 data analyzed in this manuscript have been contributed to CMIP6 and are freely available at the Earth System Grid Federation (https://esgf-node.llnl.gov/search/cmip6/) or from the NCAR Digital Asset Services Hub (DASH; https://data.ucar.edu) or from the links provided from the CESM website at: www.cesm.ucar.edu. The climatological snow data are available at: https://doi.org/10.7265/N5MS3QNJ. The IMB data are available at: http://imb-crrel-dartmouth.org. The snow radar data are available at: https://doi.org/10.5067/FAZTWP500V70, processed, and made available courtesy of Dr. Ron Kwok. ATLAS/IC-ESat-2 L3A Sea Ice Freeboard, Version 2 (ATL10) are publicly available at: https://nsidc.org/data/ATL10/versions/2. Sea ice concentration data are publicly available from the Sea Ice Index Version three at: https://nsidc.org/data/G02135/versions/3. The derived snow depth data from ICESat-2 and CryoSat-2 are available on Pangaea at: https://doi.org/10.1594/PANGAEA.914565.

References

Bacmeister, J. T., Hannay, C., Medeiros, B., Gettelman, A., Neale, R., Fredriksen, H. B., et al. (2020). CO_2 increase experiments using the Community Earth System Model (CESM): Relationship to climate sensitivity and comparison of CESM1 to CESM2. *Journal of Advances in Modeling Earth System*, *12*, e2020MS002120. https://doi.org/10.1029/2020MS002120

Bailey, D. A., Holland, M. M., DuVivier, A. K., Hunke, E. C., & Turner, A. K. (2020). Impact of a New Sea Ice thermodynamic formulation in the CESM2 Sea Ice component. *Journal of Advances in Modeling Earth Systems*, *12*, e2020MS002154. https://doi.org/10.1029/2020MS002154

Barnhart, K. R., Miller, C. R., Overeem, I., & Kay, J. E. (2015). Mapping the future expansion of Arctic open water. *Nature Climate Change*, *6*(3), 280–285. https://doi.org/10.1038/nclimate2848

Bintanja, R., & Andry, O. (2017). Towards a rain-dominated Arctic. *Nature Climate Change*, *7*, 263–267.

Blanchard-Wrigglesworth, E., S. L. Farrell, T. Newman, & C. M. Bitz (2015), Snow cover on Arctic sea ice in observations and an Earth System Model, *Geophysical Research Letters*, *42*, 10342–10348, https://doi.org/10.1002/2015GL066049

Danabasoglu, G., Lamarque, J. F., Bachmeister, J., Bailey, D. A., DuVivier, A. K., Edwards, J., et al. (2020). The Community Earth System Model version 2 (CESM2). *Journal of Advances in Modeling Earth Systems*, *12*, e2019MS001916. https://doi.org/10.1029/2019MS001916

DeRepentigny, P., Jahn, A., Holland, M. M., & Smith, A. (2020). Arctic sea ice in the two Community Earth System Model version 2 (CESM2) configurations during the 20th and 21st centuries. *Journal of Geophysical Research: Oceans*, *125*, e2020JC016133. https://doi.org/10.1029/2020JC016133

DuVivier, A., DeRepentigny, P., Holland, M., Webster, M., Kay, J., & Perovich, D. (2020). Going with the floe: Tracking CESM Large Ensemble sea ice in the Arctic provides context for ship-based observations. *The Cryosphere*, *14*(4), 1259–1271. https://doi.org/10.5194/tc-14-1259-2020

DuVivier, A. K., Holland, M. M., Kay, J. E., Tilmes, S., Gettelman, A., & Bailey, D. (2020). Arctic and Antarctic sea ice state in the Community Earth System Model Version 2. *Journal of Geophysical Research: Oceans*, *125*, e2019JC015934. https://doi.org/10.1029/2019JC015934

Fetterer, F., K. Knowles, W. N. Meier, M. Savoie, & A. K. Windnagel (2017) *Sea Ice Index, Version 3*: Boulder, Colorado USA. NSIDC: National Snow and Ice Data Center. https://doi.org/10.7265/N5K072F8

Gettelman, A., Mills, M. J., Kinnison, D. E., Garcia, R. R., Smith, A. K., Marsh, D. R., et al. (2019). The whole atmosphere community climate model version 6 (WACCM6). *Journal of Geophysical Research: Atmosphere*, *124*(23), 12380–12403. https://doi.org/10.1029/2019JD030943

Hezel, P. J., Zhang, X., Bitz, C. M., Kelly, B. P., & Massonnet, F. (2012). Projected decline in spring snow depth on Arctic sea ice caused by progressively later autumn open ocean freeze-up this century. *Geophysical Research Letters*, *39*, L17505. https://doi.org/10.1029/2012GL052794

Holland, M. M., Bailey, D. A., Briegleb, B. P., Light, B., & Hunke, E. (2012). Improved sea ice shortwave radiation physics in CCSM4: the impact of melt ponds and aerosols on arctic sea ice. *Journal of Climate*, *25*, 1413–1430.

Holland, M. M., Finnis, J., Barrett, A. P., & Serreze, M. C. (2007). Projected changes in Arctic Ocean freshwater budgets. *Journal of Geophysical Research*, *112*, G04S55. https://doi.org/10.1029/2006JG000354

Holland, M. M., & Landrum, L. (2015). Factors affecting projected Arctic surface shortwave heating and albedo change in coupled climate models. *Philosophical Transactions of the Royal Society A: Mathematical, Physical and Engineering Sciences*, *373*, 20140162. https://doi.org/10.1098/rsta.2014.0162

Hunke, E. C., & Dukowicz, J. K. (2002). The elastic–viscous–plastic sea ice dynamics model in general orthogonal curvilinear coordinates on a sphere—Incorporation of metric terms. *Monthly Weather Review*, *130*, 1848–1865.

Hunke, E. C., Hebert, D. A., & Lecomte, O. (2013). Level-ice melt ponds in the Los Alamos sea ice model, CICE. *Ocean Modelling*, *71*(26), 42. https://doi.org/10.1016/j.ocemod.2012.11.008

Hunke, E. C., & Lipscomb, W. H. (2008). *CICE: The Los Alamos sea ice model, documentation and software, version 4.0*. Los Alamos National Laboratory Tech. Rep. LA-CC-06-012.

Hunke, E. C., Lipscomb, W. H., Turner, A. K., Jeery, N., & Elliot, S. (2015). *CICE: The Los Alamos Sea ice model documentation and software users manual version 5.1 (Tech. Rep. No. LA-CC-06-012)*. Los Alamos National Laboratory.

Hurrell, J. W., Holland, M., Gent, P., Ghan, S., Kay, J. E., Kushner, P., et al. (2013). The community earth system model: A framework for collaborative research. *Bulletin of the American Meteorological Society*, *94*, 1339–1360.

Jahn, A., Kay, J. E., Holland, M. M., & Hall, D. M. (2016). How predictable is the timing of a summer ice-free Arctic?. *Geophysical Research Letters*, *43*(17), 9113–9120. https://doi.org/10.1002/2016GL070067

Kay, J. E., Deser, C., Phillips, A., Mai, A., Hannay, C., Strand, G., et al. (2015). The Community Earth System model (CESM) large ensemble project: A community resource for studying climate change in the presence of internal climate variability. *Bulletin of the American Meteorological Society*, *96*(8), 1333–1349. https://doi.org/10.1175/BAMS-D-13-00255.1

Koenig, L., Martin, S., Studinger, M., & Sonntag, J. (2010). Polar airborne observations fill gap in satellite data. *Eos*, *91*, 333–334.

Kurtz, N., & Farrell, S. (2011). Large-scale surveys of snow depth on Arctic sea ice from Operation IceBridge. *Geophysical Research Letters*, *38*, L20505. https://doi.org/10.1029/2011GL049216

Kwok, R., & Cunningham, G. F. (2015). Variability of Arctic sea ice thickness and volume from CryoSat-2. *Philosophical Transactions of the Royal Society A: Mathematical, Physical & Engineering Sciences*, *373*, 2045. https://doi.org/10.1098/rsta.2014.0157

Kwok, R., Cunningham, G. F., Kacimi, S., Webster, M. A., Kurtz, N. T., & Petty, A. (2020). Decay of the snow cover over Arctic sea ice from ICESat-2 acquisitions during summer melt in 2019. *Geophysical Research Letters*, *47*(12), e2020GL088209. https://doi.org/10.1029/2020GL088209

Kwok, R., Cunningham, G., Markus, T., Hancock, D., Morison, J. H., Palm, S. P., et al. (2019). *ATLAS/ICESat-2 L3A Sea Ice Freeboard, Version 2*. Boulder, Colorado USA: NSIDC: National Snow and Ice Data Center. https://doi.org/10.5067/ATLAS/ATL10.002

Kwok, R., Kacimi, S., Webster, M. A., Kurtz, N. T., & Petty, A. A. (2020). Arctic snow depth and sea ice thickness from ICESat-2 and CryoSat-2 freeboards: a first examination. *Journal of Geophysical Research: Oceans*, *125*, 3. https://doi.org/10.1029/2019JC016008

Kwok, R., Panzer, B., Leuschen, C., Pang, S., Markus, T., Holt, B., & Gogineni, S. (2011). Airborne surveys of snow depth over Arctic sea ice. *Journal of Geophysical Research*, *116*, C11018. https://doi.org/10.1029/2011JC007371

Labe, Z., Magnusdottir, G., & Stern, H. (2018). Variability of Arctic Sea Ice Thickness Using PIOMAS and the CESM Large Ensemble. *Journal of Climate*, *31*(8), 3233–3247. https://doi.org/10.1175/JCLI-D-17-0436.1

Light, B., Dickinson, S., Perovich, D. K., & Holland, M. M. (2015). Evolution of summer Arctic sea ice albedo in CCSM4 simulations: Episodic summer snowfall and frozen summers. *Journal of Geophysical Research: Oceans*, *120*, 284–303. https://doi.org/10.1002/2014JC010149

Lique, C., Holland, M. M., Dibike, Y. B., Lawrence, D. M., & Screen, J. A. (2016). Modeling the Arctic freshwater system and its integration in the global system: Lessons learned and future challenges. *Journal Geophysical Research: Biogeoscience*, *121*, 540–566. https://doi.org/10.1002/2015JG003120

Maykut, G. A. (1978). Energy exchange over young sea ice in the central Arctic. *Journal of Geophysical Research*, *83*, 8C0241. https://doi.org/10.1029/JC083iC07p03646

McIlhattan, E. A., Kay, J. E., & L'Ecuyer, T. S. (2020). Arctic clouds and precipitation in the community Earth system model version 2. *Journal of Geophysical Research: Atmospheres*, *125*, e2020JD032521. https://doi.org/10.1029/2020JD032521

McIlhattan, E. A., L'Ecuyer, T. S., & Miller, N. B. (2017). Observational evidence linking arctic supercooled liquid cloud biases in CESM to snowfall processes. *Journal of Climate*, *30*(12), 4477–4495. https://doi.org/10.1175/JCLI-D-16-0666.1

Meehl, G. A., Arblaster, J. M., Bates, S., Richter, J. H., Tebaldi, C., Gettelman, A., et al. (2020). Characteristics of future warmer base states in CESM2. *Earth & space science*, *7*(9), e2020EA001296. https://doi.org/10.1029/2020EA001296

Nandan, V., Geldsetzer, T., Yackel, J., Mahmud, M., Scharien, R., Howell, S., et al. (2017). Effect of snow salinity on CryoSat-2 Arctic first-year sea ice freeboard measurements. *Geophysical Research Letters*, *44*(20), 10419–10426. https://doi.org/10.1002/2017GL074506

O'Neill, B. C., Tebaldi, C., van Vuuren, D. P., Eyring, V., Friedlingstein, P., Hurtt, G., et al. (2016). The Scenario Model Intercomparison Project (ScenarioMIP) for CMIP6. *Model Dev*, *9*, 3461–3482. https://doi.org/10.5194/gmd-9-3461-2016

Panzer, B., Leuschen, C., Patel, A., Markus, T., & Gogineni, S. (2010). Ultrawideband radar measurements of thickness of snow over sea ice. *IEEE Transactions on Geoscience and Remote Sensing*, *45*, 2715–2724. https://doi.org/10.1109/IGARSS.2010.5654342

Perovich, D., Richter-Menge, J. A., Elder, B., Arbetter, T., Claffey, K., & Polashenski, C. (2017a). *Observing and understanding climate change: Monitoring the mass balance, motion, and thickness of Arctic sea ice*. Retrived from https://imb-crreldartmouth.org

Perovich, D. K., Grenfell, T. C., Light, B., & Hobbs, P. V. (2002). Seasonal evolution of the albedo of multiyear Arctic sea ice. *Journal of Geophysical Research*, *107*(C10), 8044. https://doi.org/10.1029/2000JC000438

Perovich, D. K., & Polashenski, C. (2012). Albedo evolution of seasonal Arctic sea ice. *Geophysical Research Letters*, *39*, L08501. https://doi.org/10.1029/2012GL051432

Perovich, D., Polashenski, C., Arntsen, A., & Stwertka, C. (2017b). Anatomy of a late spring snowfall on sea ice. *Geophysical Research Letters*, *44*, 2802–2809. https://doi.org/10.1002/2016GL071470

Petrich, C., Eicken, H., Polashenski, C. M., Sturm, M., Harbeck, J. P., Perovich, D. K., & Finnegan, D. C. (2012). Snow dunes: A controlling factor of melt pond distribution on Arctic sea ice. *Journal of Geophysical Research*, *117*, C09029. https://doi.org/10.1029/2012JC008192

Provost, C., Sennéchael, N., Miguet, J., Itkin, P., Rösel, A., Koenig, Z., et al. (2017). Observations of flooding and snow-ice formation in a thinner Arctic sea-ice regime during the N-ICE2015 campaign: influence of basal ice melt and storms. *Journal of Geophysical Research: Oceans*, *122*(9), 7115–7134. https://doi.org/10.1002/2016JC012011

Radionov, V. F., Bryazgin, N. N., Alexandrov, E. I., & Tech (1997). *The snow cover of the arctic Basin*. Lab Report. APL-UW-TR 9701 (pp. 95). Seattle: Washington University Seattle Applied Physics Lab.

Sturm, M., & Massom, R. A. (2017). *Sea Ice 65–109*. Oxford: Wiley and Blackwell.

Sturm, M., Perovich, D. K., & Holmgren, J. (2002). Thermal conductivity and heat transfer through the snow on the ice of the Beaufort Sea. *Journal of Geophysical Research*, *107*(C21), 8043. https://doi.org/10.1029/2000JC000409

Turner, A. K., Hunke, E. C., & Bitz, C. M. (2013). Two modes of sea-ice gravity drainage: A parametrization for large-scale modeling. *Journal of Geophysical Research*, *118*(5), 2279–2294. https://doi.org/10.1002/jgrc.20171

van Vuuren, D. P., Edmonds, J., Thomson, A., Riahi, K., Kainuma, M., Matsui, T., et al. (2011). The representative concentration pathways: An overview. *Climatic Change*, *109*(5–31), 5.

Warren, S. G., Rigor, I., Untersteiner, N., Radionov, V. F., Bryazgin, N. N., Aleksandrov, Y. I., et al. (1999). Snow depth on Arctic sea ice. *Journal of Climate*, *12*, 1814–1829.

Webster, M. A., Rigor, I., Nghiem, S. V., Kurtz, N., Farrell, S. L., Perovich, D. K., et al. (2014). Interdecadal changes in snow depth on Arctic sea ice. *Journal of Geophysical Research: Oceans*, *119*, 5395–5406.

Webster, M. A., Gerland, S., Holland, M., Hunke, E., Kwok, R., Lecomte, O., et al. (2018). Snow in the changing sea-ice systems. *Nature Climate Change*, *8*, 946–953.

Webster, M. A., Parker, C., Boisvert, L., & Kwok, R. (2019). The role of cyclone activity in snow accumulation on Arctic sea ice. *Nature Communications*, *10*(1), 5285. https://doi.org/10.1038/s41467-019-13299-8

Webster, M. A., Rigor, I. G., Perovich, D. K., Richter-Menge, J. A., Polashenski, C. M., & Light, B. (2015). Seasonal evolution of melt ponds on Arctic sea ice. *Journal of Geophysical Research: Oceans*, *120*, 5968–5982. https://doi.org/10.1002/2015JC011030